



## Comparative study of catalytic performance and degradation kinetics of biodiesels produced using heterogeneous catalysts from kaolinite

Faisal Abnisa<sup>a,\*</sup>, Samuel Eshorame Sanni<sup>b</sup>, Peter Adeniyi Alaba<sup>c</sup>

<sup>a</sup> Department of Chemical and Materials Engineering, Faculty of Engineering, King Abdulaziz University, Jeddah 21589, Saudi Arabia

<sup>b</sup> Department of Chemical Engineering, Covenant University, P.M.B 1023, Ota, Ogun State, Nigeria

<sup>c</sup> Chemical Engineering Department, Faculty of Engineering, University Malaya, 50603 Kuala Lumpur, Malaysia

### ARTICLE INFO

Editor: Teik Thye Lim

#### Keywords:

Catalytic process

Biodiesel

SHY zeolite

Kinetics

Alternative energy

### ABSTRACT

This study comparatively investigates the catalytic activities and degradation kinetics of the produced biodiesels using kaolinite-based heterogeneous catalysts to examine the stability. The performance of the catalysts was tested under the same operating parameter (methanol/oil ratio, 5:1, at 200 °C for 6 h). The obtained biodiesel was analyzed using TGA equipment to obtain the yield, as well as the degradation kinetic parameters. It was observed that the solid superacid SHY zeolite gave the highest biodiesel yield (90.76%) because of higher acid strength. The catalysts performance is in the order of HY < ALK < HLK < NaLK < SHY zeolite. The lower performance of HY (72.42% yield) is attributed to the presence of high basic sites, being that shea butter has high FFA. The degradation kinetics of each biodiesel sample was performed using the TGA data to examine the thermal and oxidative stability. The frequency factor (A), activation energy, and reaction order were determined by employing the Coats-Redfern model. It was observed that first-order reaction mechanism can satisfactorily describe all the biodiesel kinetics. Further, the biodiesel from SHY zeolite gives the highest  $E_A$  (98.65 kJ/mol). This result indicates that SHY zeolite is the best catalyst in terms of biodiesel yield and stability.

### 1. Introduction

The need for renewable and sustainable alternative energy sources is in high demand because the world petroleum reserve is depleting, and greenhouse gas (GHG) emissions from fossil fuel prevail. Currently, biomass fuel is a promising alternative due to environmental renewability and friendliness [1]. One of the prominent alternative energy sources bio-oil. However, bio-oil exhibits high acid value, low heating value, and high viscosity, harmful to the fuel engine. High oxygen content is majorly responsible for the poor property of bio-oil. This drawback necessitates the need to transform bio-oil to biodiesel via transesterification and esterification to enhance its quality. Biodiesel is preferred to fossil-diesel because biodiesel is biodegradable, renewable, and friendly to the environment. Interestingly, biodiesel possesses better cetane number, flash point, and lubricating property than fossil-diesel, which prolongs engine life [2,3].

Generally, transesterification reaction is carried out using homogeneous alkaline catalysts like NaOH, KOH, and inorganic alkaline [4]. The prevalence of homogeneous alkaline catalysts to solid acid catalysts

is mainly because of their superior performance [5]. Meanwhile, the use of homogeneous catalysts is plagued with various setbacks. The setbacks are difficulty in catalyst recovery, soap formation, and separation of glycerol is not cost-sensitive since a large amount of water is required, leading to wastewater production [6–8].

The application of heterogeneous catalysts like solid acids has enjoyed wide acceptance in thermocatalytic reactions like petrochemical processes and bulk chemistry due to their outstanding benefits [9]. Heterogeneous catalysts can be recovered for reuse by separation via filtration. The reusability of heterogeneous catalyst boosts its economic viability, making it considerable for industrial manufacturing processes. However, a suitable heterogeneous catalyst must be porous enough to avoid steric hindrance since the adsorption in the heterogeneously catalyzed reaction is mostly the rate-limiting step [9].

Zeolites are promising solid acids with remarkable attributes like strong acidity, high porosity, and selectivity, attracting several applications in energy industries [10,11]. Zeolites like Y and ZSM-5 have an excellent porosity for valorization biomass, including bio-oil into biodiesel. Zeolites have controlled pore openings and internal pore space,

\* Corresponding author.

E-mail addresses: [fta@kau.edu.sa](mailto:fta@kau.edu.sa), [faisal.abnisa@gmail.com](mailto:faisal.abnisa@gmail.com) (F. Abnisa), [samuel.sanni@covenantuniversity.edu.ng](mailto:samuel.sanni@covenantuniversity.edu.ng) (S.E. Sanni), [adeniyipee@live.com](mailto:adeniyipee@live.com) (P.A. Alaba).

<https://doi.org/10.1016/j.jece.2021.105569>

Received 25 January 2021; Received in revised form 17 April 2021; Accepted 20 April 2021

Available online 29 April 2021

2213-3437/© 2021 Elsevier Ltd. All rights reserved.

**Table 1**  
Properties of crude shea butter.

Properties	Shea butter	Biodiesel
Density ( $\text{kg m}^{-3}$ ) at 25 °C	0.91	0.87
Viscosity ( $\text{mm}^2 \text{s}^{-1}$ ) at 38 °C	39.98	3.47
Flashpoint (°C)		164.4
HHV ( $\text{MJ kg}^{-1}$ )		41.3
Cetane number		52
Acid value	3.62	
Iodine value ( $\text{I}_2 \text{ g } 100 \text{ g}^{-1}$ )	59.5	
Saponification value ( $\text{mg KOH g}^{-1}$ )	190	
Peroxide value ( $\text{meq O}_2 \text{ kg}^{-1}$ )	12.15	
Water content (wt%)	0.037	
Fatty acid composition (%)		
Palmitic (C16:0)	5.4	
Stearic (C18:0)	35.7	
Oleic (C18:1)	49.6	
Linoleic (C18:2)	7.8	
Arachidic (C20:0)	1.3	

preventing coke formation [12,13]. However, zeolites suffer mass transfer limitation, making them unsuitable for the reaction of bulky molecules. The reaction of these molecules can only occur at the external surface of zeolites, which accounts for a smaller percentage of the material. Furthermore, the external surface does not have sufficient active sites for efficient transformation of bulky reactants [12]. Hierarchical ZSM-5 zeolite is a variant of ZSM-5 that can improve bulky molecule conversion and produce high aromatics yield [14,15].

Moreover, biodiesels are less stable compared to conventional diesel. Biodiesels are susceptible to oxidation due to environmental factors like light, air, moisture, etc. Biodiesel transforms to undesirable smaller chain composites like small chain esters, aldehydes, etc., during oxidation [16]. The oxidation process reduces the fuel quality, leading to problems like choking of fuel filter and injector and forming deposits in the combustion chamber. Factors responsible for the instability of biodiesel include polyunsaturation [17], the number of bis-allylic sites [18], and the position of the C–C double bond [16]. Several authors have worked on the stability of biodiesels [16,19,20]. Therefore, it is crucial to make a frantic effort to produce biodiesel with good stability.

The high cost of heterogeneous catalysts is the major challenge preventing heterogeneous catalysis from attaining biodiesel production prominence. Therefore, the search for a cost-effective precursor with equally remarkable catalytic properties is necessary to alleviate the economic limitations. Clay minerals like kaolinite enjoy industrial utilizations catalysts in the last decades. Kaolinites have been an active catalyst precursor in several industrial processes like petrochemistry, particularly in bulk chemistry and catalytic refining. The popularity of kaolinites could be ascribed to their remarkable pore size and structure, suitable for transforming bulky molecules [21]. These features are the main reason for the ever-increasing attention to aluminosilicates from clay towards solid acid catalyst synthesis.

Meanwhile, kaolinite can withstand acid leaching during activation since it contains high octahedral alumina. This resistance can be subdued by calcination at 550–950 °C temperatures range, transforming the clay into metakaolin. However, the crystalline structure of the clay material will be deformed.

Interestingly, the industrial applications of kaolinite-based catalysts have been reported since the early 1930s. Notable progress in several industrial processes like petrochemistry; specifically, in bulk chemistry and catalytic refining, is made feasible with kaolinite as the starting material in the synthesis of active catalyst. The catalytic utilization of kaolinites is attributed to their unique pore size and structure, facilitating bulky molecule conversion [22]. These engendered a renewed interest in clay-generated aluminosilicates for zeolites synthesis. Therefore, this study comparatively explored the stability of biodiesel produced using different catalysts prepared using kaolinite as a precursor. The synthesized catalysts include mesoporous aluminosilicates,

mesoporous HY zeolites, and sulfated HY. The biodiesel precursor used is shea butter. Shea butter is an ivory-colored fat produced from shea nut of *Vitellaria paradoxa*, a sub-Saharan African shea tree with high free fatty acid (FFA) content, mainly unsaturated triglyceride (Oleic (C18:1) and Linoleic (C18:2)) [23], which often induces oxidative instability in the produced biodiesel. Our previous work [24] has reported the viability of kaolin-based catalyst for biodiesel production from shea butter based on its remarkable activity and reusability. The properties of crude shea butter are presented in Table 1 [23]. The performance and kinetics of all the prepared catalysts were comparatively studied to examine the yield and stability of the biodiesels.

## 2. Materials and method

### 2.1. Materials

The kaolin, ZSM-5 zeolite,  $\text{H}_2\text{SO}_4$  (95–98% pure), NaOH,  $\text{NH}_4\text{NO}_3$  (99.0%), and 99.9% methanol (MeOH) used were supplied by R&M Chemicals Sdn. Bhd., Malaysia. The reagents were used as received. The shea butter was purchased from Ikotun, Lagos, Nigeria, and was subjected to 110 °C in the oven to remove moisture.

### 2.2. Modified kaolinite

The kaolin was calcined at 850 °C to form metakaolin, which has lesser impurities and more susceptible to dealumination. The metakaolin was leached using 6 M  $\text{H}_3\text{PO}_4$  for 4 h at 90 °C. After the leaching, the resulting sample was divided into two, after which a part was quenched with distilled water and washed continuously with distilled water until the pH value becomes 5. The second part of the sample was mixed with a particular concentration of aqueous NaOH (14 wt%) until the pH value of 5 is attained. The two solutions were screened using a vacuum pump and dried overnight at 120 °C. The samples washed with demineralized water, and aqueous NaOH (14 wt%) for pH regulation were denoted as ALK and NaLK, respectively. The NaLK sample was treated for 24 h with 0.1 M  $\text{NH}_4\text{NO}_3$  to transform it to its hydronium form. The resulting samples were filtered and dried at 120 °C for 12 h and named HLK. All the samples are subjected to calcination at 550 °C for 2 h.

### 2.3. Hierarchical nanoporous HY zeolite

The synthesized ALK was used as the precursor for the synthesis of HY zeolites. ALK was added to an aqueous solution of NaOH (14 wt%). The solution was subjected to ageing at room temperature for 24 h followed by crystallization for 24 h at 100 °C. The obtained sample was rinsed with distilled water and filtered using powered by a vacuum pump till a pH below 9 is reached. The resulting sample was dried for 12 h at 110 °C prior to soaking in a NaCl saturated solution for 2 h [25]. The sample was treated for 24 h with 0.2 M  $\text{NH}_4\text{NO}_3$  to transform it to its hydronium form. The resulting sample was filtered and dried at 110 °C overnight and subsequent calcination for 2 h at 550 °C.

### 2.4. Sulfated HY zeolite (SHY)

The prepared HY zeolite was incipiently impregnated with  $\text{H}_2\text{SO}_4$  to produce sulfated HY [26] zeolite. The impregnation was carried out by adding 5 g of the HY to 50 mL of 1 M  $\text{H}_2\text{SO}_4$  solution. The mixture was thoroughly mixed at ambient temperature for 1 h. The resulting sample, SHY was dried in an oven for 24 h and calcined at 450 °C for 3 h.

### 2.5. Characterization

The samples were analyzed using X-ray diffraction analysis (XRD) PANanalytical X'pert Empyrean X-ray diffractometer with  $\text{CuK}\alpha$  radiation at 40 kV and 40 mA. The mean crystallite size and crystallinity were

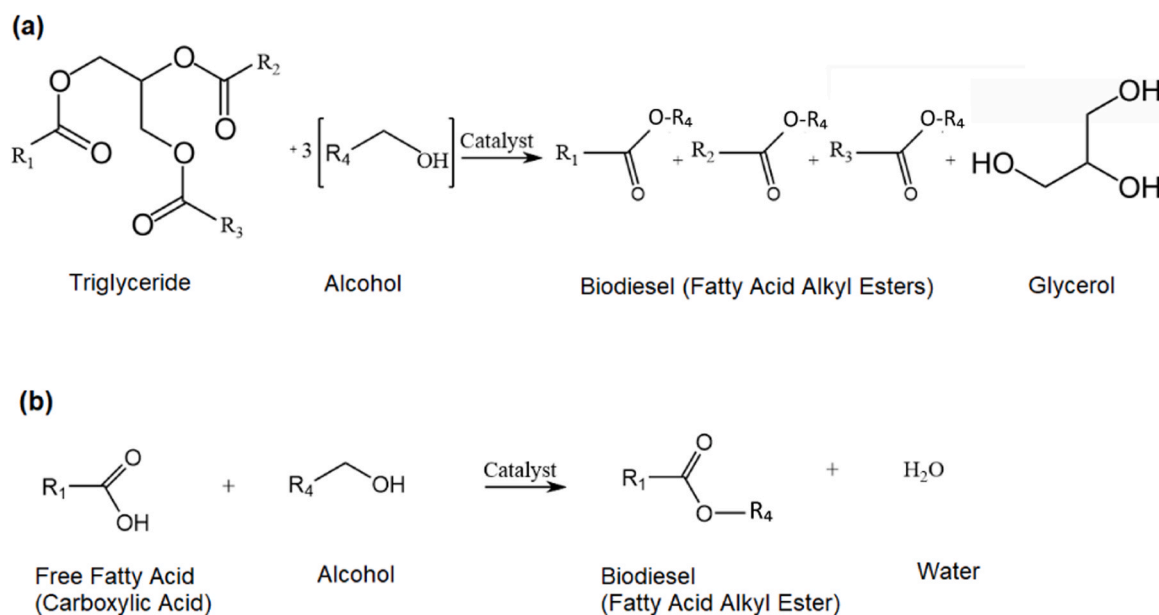


Fig. 1. Schematic diagram for (a) transesterification and (b) esterification reactions.

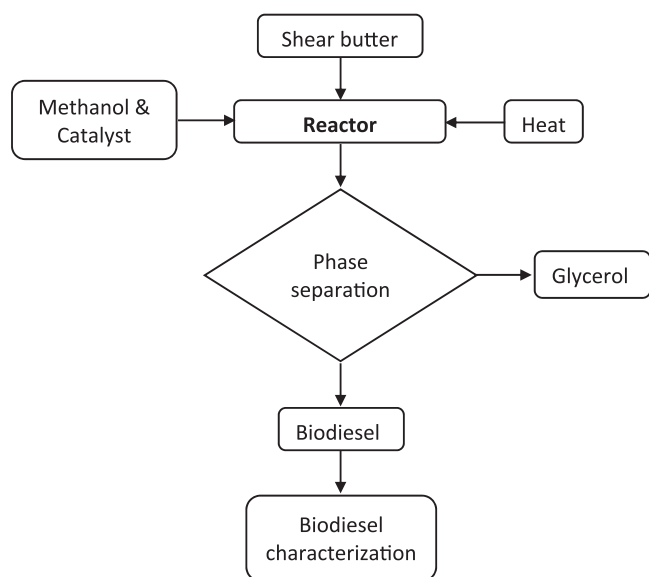


Fig. 2. Schematic diagram of the experimental setup for biodiesel production.

determined using the characteristic reflection peaks [25]. The crystal size of the peaks mentioned above was determined using PANalytical X'Pert HighScore [23].

The samples' functional groups were examined using FTIR with the aid of Perkin Elmer Spectrum RX FT-IR.  $N_2$  adsorption-desorption isotherms were analyzed using porosity and surface area analyzer (Micrometrics ASAP 2020) using 77.350 K as the analysis bath temperature. The samples were outgassed for 2 h at 130 °C before each measurement for the sake of accuracy. Brunauer–Emmett–Teller [27] and t-plot technique were used to examine the pore-size distribution, microporous volume, microporous area, and specific surface area.

## 2.6. Catalytic performance

The performance of the catalysts was evaluated during the production of biodiesel from shea butter. The process was performed using surplus methanol in an airtight stainless steel autoclave reactor. Figs. 1

and 2 present the schematic representation of biodiesel production. The reaction was done at 200 °C with 5:1 alcohol/oil molar ratio and 1 wt% catalyst loading for 6 h. After the reaction, the glycerol and unreacted shea butter were separated using a separation funnel. The selection of the operating parameters is based on our previous studies [23,24].

Moreover, the samples were analyzed using TGA to determine the biodiesel yield. The TG analysis of the produced biodiesels and shea butter was done by adding a certain amount of the sample to the crucible. The analysis was done in a nitrogen atmosphere at a temperature range of 50–500 °C and 20 °C/min as the heating rate.

TGA is a cost-effective and fast technique for quantitative analysis of a mixture of materials [23]. Several authors have confirmed that the determination of biodiesel yield using TGA could be compared with GC method [2,23,28]. Chand et al. [28] compared TGA with GC, proton NMR, and HPLC technique in determining biodiesel yield of transesterified oil. The report shows that the TGA results could be compared with those of GC proton NMR, and HPLC. The efficacy of TGA technique could be compared with  $^1\text{H}$ NMR technique within  $\pm 1.5\%$ .

## 2.7. Computation of kinetic parameters

Kinetic study of the pyrolysis process is complicated because of the occurrence of several reactions, both in parallel and series [29]. Mainly, the degradation rate is

$$\frac{dx}{dt} = k(T)f(x)^n \quad (1)$$

Where the degree of conversion is denoted by  $x$ ,  $T$ , and  $t$  represents temperature and time, respectively. The rate of conversion  $\frac{dx}{dt}$  for pyrolysis at a constant heating rate,  $\beta = \frac{dT}{dt}$ , is given by;

$$\frac{dx}{dt} = \beta \frac{dx}{dT} = k(T)f(x) \quad (2)$$

Moreover, the conversion,  $x$  is;

$$x = \frac{w_0 - w}{w_0 - w_f} \quad (3)$$

Where  $w$ ,  $w_0$ , and  $w_f$  refers to sample weights at time  $t$ , at the beginning and end, respectively. Arrhenius equation is often used to model  $k(T)$  because weight loss is temperature-dependent [29,30].

**Table 2**  
Algebraic expressions of functions of the most common reaction mechanism [29].

Mechanism	f(x)	g(x)
Power law	$2x^{1/2}$	$x^{1/2}$
Power law	$3x^{2/3}$	$x^{1/3}$
Power law	$4x^{3/4}$	$x^{1/4}$
One dimensional diffusion model	$\frac{1}{2}x$	$x^2$
Two-dimensional diffusion model	$[-\ln(1-x)]^{-1}$	$[(1-x)\ln(1-x)]+x$
Three-dimensional diffusion model	$\frac{3(1-x)^{2/3}}{[2(1-(1-x)^{1/3})^3]}$	$1-(2x/3)-(1-x)^{2/3}$
First-order reaction model	$(1-x)$	$-\ln(1-x)$
Second-order reaction model	$(1-x)^2$	$(1-x)^{-1}-1$
Third-order reaction model	$(1-x)^3$	$[(1-x)^{-2}-1]/2$

$$k(T) = A \exp\left(-\frac{E_A}{RT}\right) \tag{4}$$

where the gas constant is represented by R (8.314 J/mole K), frequency factor, A ( $\text{min}^{-1}$ ), activation energy,  $E_A$  (kJ/mol) and absolute temperature, T (K). Combining Eqs. (1) and (2) we have;

$$\beta \frac{dx}{dT} = A \exp\left(-\frac{E_A}{RT}\right) f(x) \tag{5}$$

Coats-Redfern kinetic models were used to analyze the TG data.

Coats and Redfern [31] formulated an integral model, suggesting that a suitable order produces the best straight-line plot. Hence, Eq. (5) can be written as:

$$\ln\left(\frac{g(x)}{T^2}\right) = \ln\left(\frac{AR}{\beta E_A}\right) - E_A / (RT) \tag{6}$$

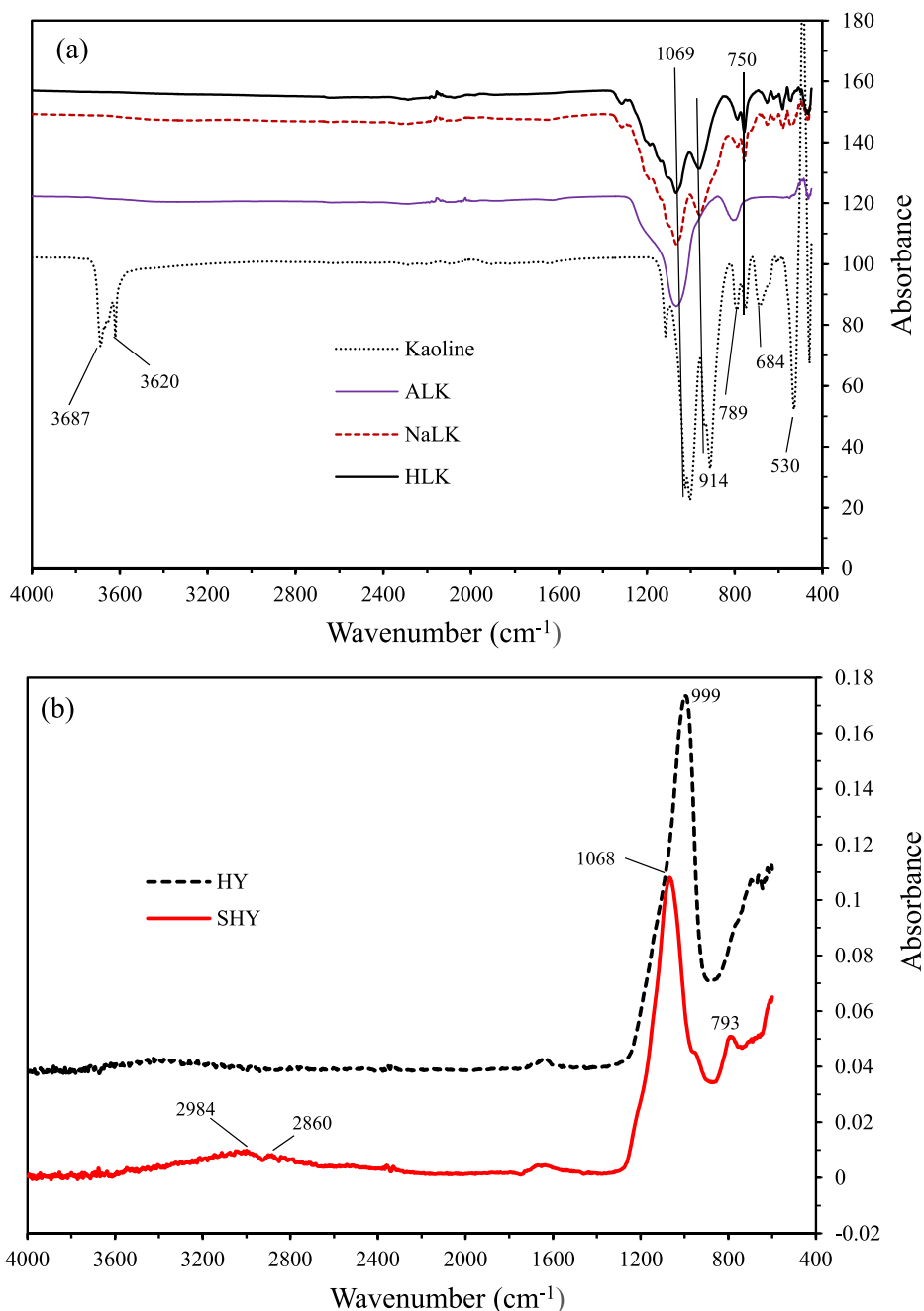


**Fig. 3.** FTIR spectra of untreated kaolin and synthesized kaolinites.

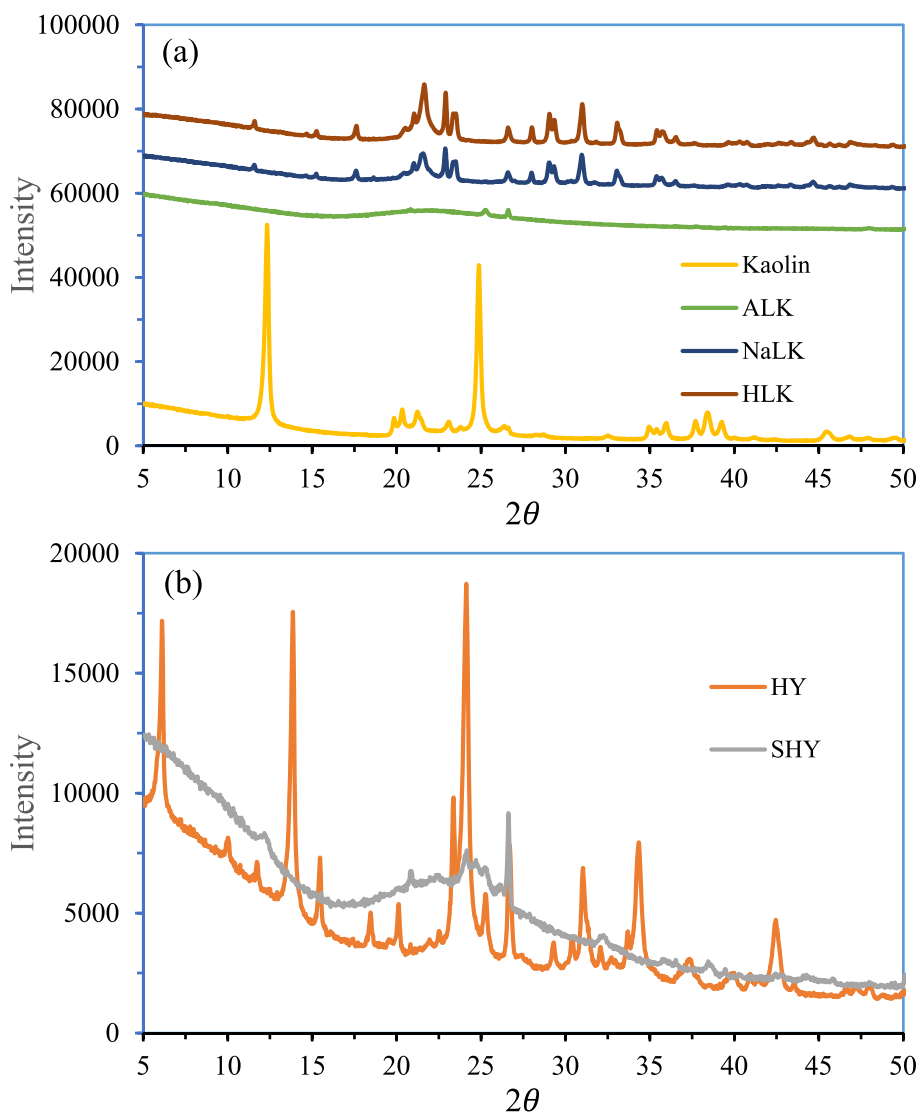


Fig. 4. XRD pattern of the synthesized catalysts.

The plot of  $\ln(g(x)/T^2)$  vs.  $1/T$  gives a linear plot whose intercept is  $\ln(AR/\beta E_A)$ , and the slope is equal to  $-E_A/R$ . Hence, the value of  $E_A$  and  $A$  is determined. The values of the function  $g(x)$  are presented in Table 2. The mechanism was explored using first, second and third-order reaction model.

### 3. Results and discussion

#### 3.1. FTIR analysis

Fig. 3 presents FTIR bands of unmodified kaolinite and that of modified samples. The unmodified kaolinite spectrum shows unusual bands at 3620, 3632, and 3687  $\text{cm}^{-1}$  in the region of O-H stretching, corresponding to the octahedral OH units ( $\text{Al-OH}_{\text{str}}$ ) (Fig. 1a) [32,33]. The 3687  $\text{cm}^{-1}$  bands showed a strong inner surface O-H in-phase vibration stretching. In the same vein, the 3620  $\text{cm}^{-1}$  absorption band exhibits a strong inner surface O-H vibration stretching between the octahedral and tetrahedral lamella of kaolinite [32,34]. On the other hand, the 3632  $\text{cm}^{-1}$  inner surface OH vibration stretching at the out-phase has medium strength [25]. After calcination at 850  $^{\circ}\text{C}$ , the unique bands were no more. This phenomenon is ascribed to the cleavage of hydrogen bonds between the kaolinite layers because of the effect of temperature on the structural hydroxyl units. The thermal effect

enables more severe leaching of the clay by the acid [35]. Similarly, kaolinite exhibits bending regions at 530, 684, 750, 789, and 914  $\text{cm}^{-1}$  vanished after calcining and acid attack (Fig. 3b). This engenders structural defects on the kaolinite from crystalline to amorphous structure. This agrees with the XRD data presented in Fig. 2. The vanishing is despite the varying vibrational directions of 530 and 914  $\text{cm}^{-1}$  bands ( $\text{Si-OH}$  and  $\text{Al-OH}$  vibrations bending) and 684, 750, and 789  $\text{cm}^{-1}$  bands, which represent  $\text{Al-OH}$  ("gibbsite-like" layer) translational vibrations [35]. These bands resurfaced at the bending region, as shown by produced NaLK samples. This transformation could be attributed to the restoration of the crystalline structure in the sample. On the other

Table 3  
Textural properties of the samples.

Sample	$S_{\text{BET}}$ $\text{m}^2/\text{g}$	$S_{\text{micro}}^{\text{a}}$ $\text{m}^2/\text{g}$	$S_{\text{meso}}^{\text{a}}$ $\text{m}^2/\text{g}$	$V_{\text{total}}^{\text{a}}$ $\text{cm}^3/\text{g}$	$V_{\text{mic}}^{\text{a}}$ $\text{cm}^3/\text{g}$	$D_{\text{meso}}^{\text{b}}$ (nm)
ALK	408.19	33.21	374.98	0.348	0.0088	4.96
HLK	1.81	0.35	1.45	0.006	0.0001	30.38
NaLK	2.75	0.39	2.36	0.010	0.0001	24.51
HY Zeolite	443.78	363.24	80.55	0.23	0.1435	2.08
SHY Zeolite	65.81	16.91	48.9	0.063	0.0077	3.84

<sup>a</sup> Calculated from the t-plot curve.

<sup>b</sup> BJH method.

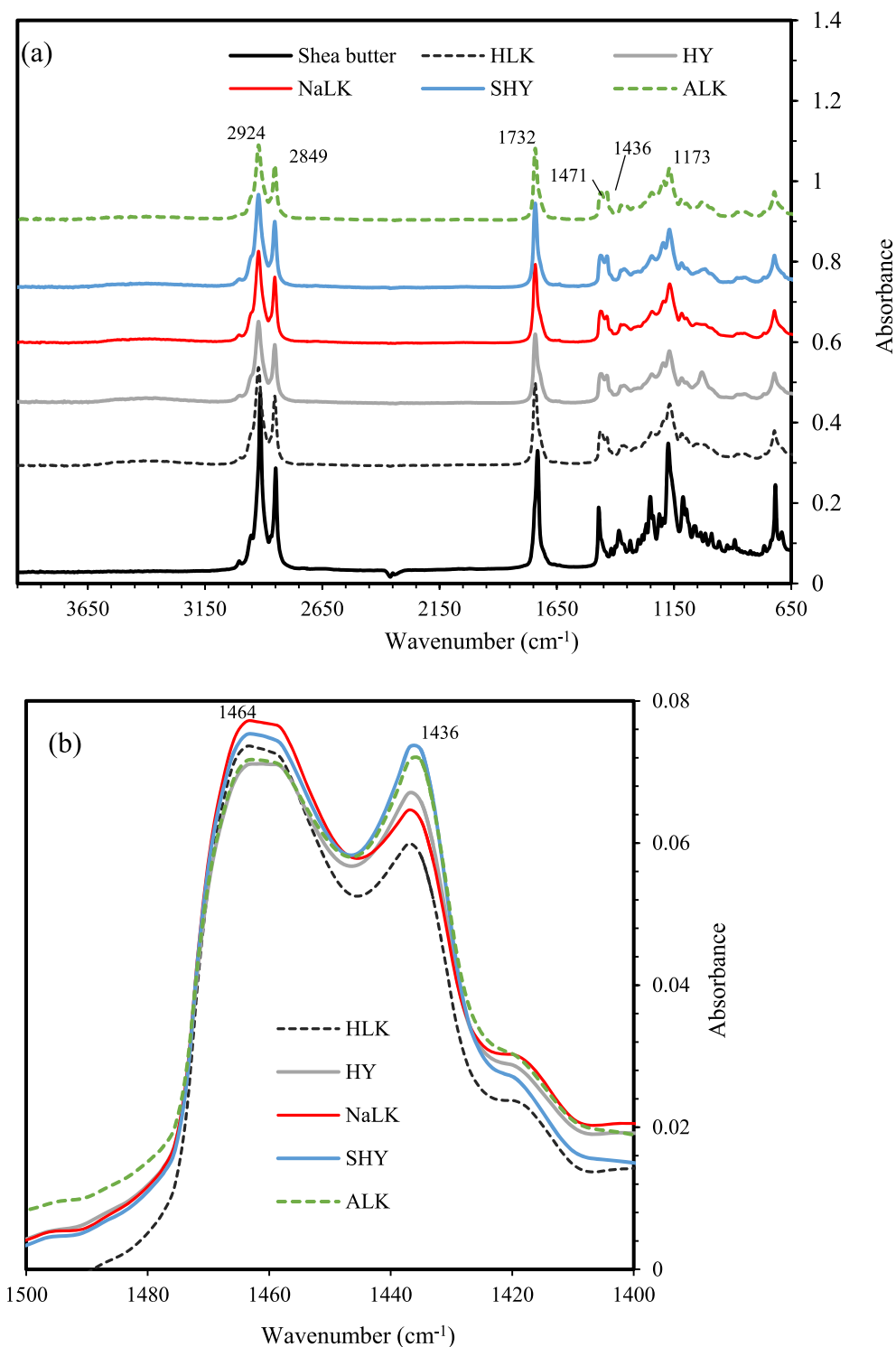


Fig. 5. FTIR confirming the formation of biodiesel from shea butter.

hand, since the Si/Al ratio increases, the peak intensities of NaLK become lower than that of the unmodified kaolinite.

The FTIR spectra in Fig. 3b show the presence of sulfate ions on SHY located at 792.53, 950, and 1067.97  $\text{cm}^{-1}$  which could be ascribed to the asymmetric and symmetric stretching vibration of  $\text{S}^=\text{O}$  and  $\text{S}-\text{O}$  bonds being sulfate of the inorganic chelating bidentate. However, the band at 1067.97  $\text{cm}^{-1}$  overlapped the HY band at 998.97  $\text{cm}^{-1}$ . In comparison to HY, SHY spectrum exhibited two broad peaks at 2860.32 and 2983.75  $\text{cm}^{-1}$  which are ascribed to  $\text{CH}_2$  asymmetric stretching

vibration.<sup>34</sup> The  $\text{S}^=\text{O}$  bond, due to its partial ionic nature, boosted the Bronsted acid sites of the zeolite. The observations reveal that sulfate groups were effectively attached to the surface of SHY.

### 3.2. X-ray diffractograms analysis

Several studies [22,36,37] have revealed that it is possible to detect major variances like crystallinity index for various kaolinites in the range of  $20^\circ < 2\theta > 24^\circ$ . Transforming kaolinite to metakaolin after 2 h at

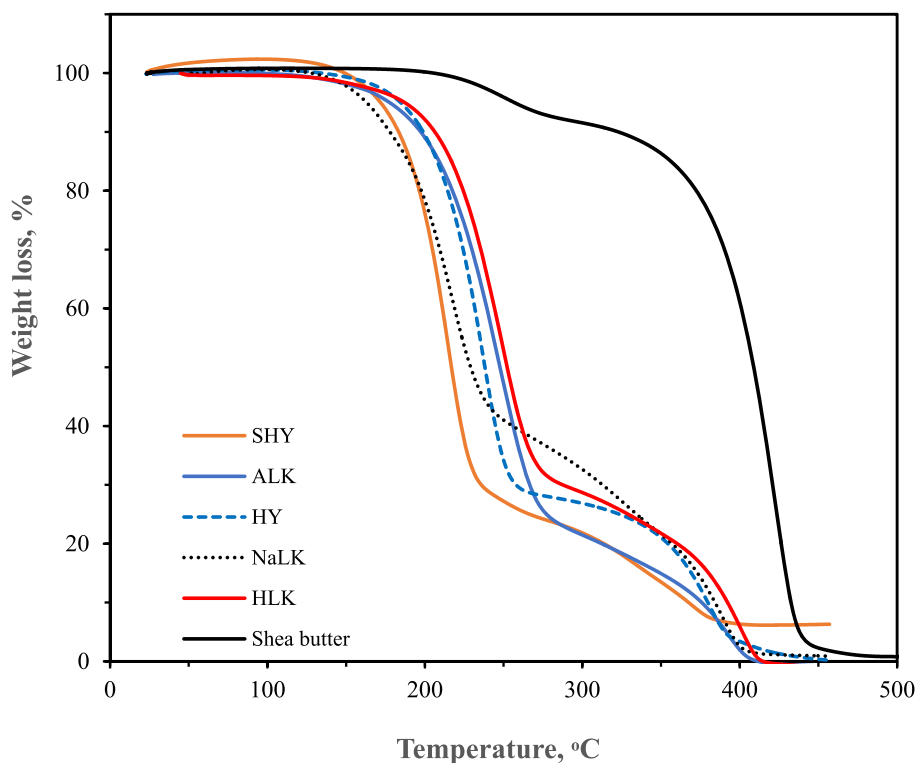


Fig. 6. TG curves of shea butter and biodiesel sample.

850 °C leads to the disappearance of all the kaolinite peaks and loss of water. On the other hand, the attachment of quartz and anatase ( $\text{TiO}_2$ ) substitutes the peaks with a broadband peak within  $20^\circ < 2\theta > 30^\circ$ . This could be ascribed to the increase in anatase composition and the presence of amorphous  $\text{SiO}_2$  [22]. This is revealed by the presence of three peaks at  $55^\circ$ ,  $48^\circ$  and  $26.61^\circ$  (Fig. 4a). However, the departure of the peak at 001 basal planes ( $2\theta$ ) could be ascribed to the cleavage of the hydrogen bonds between the kaolinite layers. The structural water loss transformed the coordination of the alumina unit to Penta- and tetrahedral form octahedral structure [35]. Furthermore, it makes kaolinite susceptible to acid leaching by partial leaching of  $\text{Al}^{3+}$ . As a result, the acid-modified kaolinite (ALK) shows the same XRD spectrum as meta-kaolin, although the amorphous phase increased. However, the XRD spectrum of conventional kaolinite exhibits characteristic peaks at  $2\theta$  values of  $12.34^\circ$  and  $24.87^\circ$  (Fig. 4a). The XRD spectrum of the NaOH-modified sample (NaLK) shows reappearance of the peak at 001 basal planes ( $2\theta$ ) although with a declining intensity. This trend could be attributed to the bonding of hydrogen bonds between the sample layers. However, ion exchange boosted the intensity of all the peaks, as revealed by the sample named HLK. Further, peak intensity within  $20^\circ < 2\theta > 24^\circ$  was restored.

The XRD pattern of the samples exhibits pure Y zeolite characteristic peaks ((440), (511), (533), and (642)) without impurities like MOR, P and 4A zeolite peaks. The observations reveal that all the synthesized HY zeolite has characteristic peaks of Y zeolite, although with a lower intensity. The XRD spectrum in Fig. 3b shows the transformation from HY to SHY after the acid treatment. The sample's crystallinity peaks decrease vastly by  $\sim 49.6\%$  as revealed by the characteristic peaks of Y zeolite (at  $2\theta = 18.5, 20.2, 23.5$  and  $26.8$ ). Specifically, the declined crystallinity is demonstrated by the disappearance and declining intensity of some of the characteristic peaks of Y zeolite and the reduction in the crystal size from 30.41 to 30.33 nm (Table 3).

### 3.3. $\text{N}_2$ adsorption-desorption

Table 3 gives the textural attributes of the catalyst samples. The

results reveal that the adjustment of the pH of modified kaolinite using NaOH rather than distilled water results in a drastic decline in the pore volume and specific surface area (SSA). The SSA of ALK and NaLK are  $408.2$  and  $2.7 \text{ m}^2/\text{g}$ , respectively. Moreover, modification of HY zeolite with sulfate ion results in a drastic reduction in the value of SSA (from  $444$  to  $66 \text{ m}^2/\text{g}$ ) and pore volume (from  $0.23$  to  $0.063 \text{ m}^3/\text{g}$ ). The reduction in the SSA and pore volume that resulted in NaLK and SHY catalysts is ascribed to the collapse of the walls of the mesopore, which intensely widens the pore. Moreover, ion-exchanged modified kaolinite with  $0.1 \text{ M NH}_4\text{NO}_3$  further reduces the pore volume and SSA due to the collapse of the walls of the mesopore.

### 3.4. Biodiesel confirmation

Fig. 5 presents FTIR confirmation of the yield of biodiesel using different kaolin-based catalysts. The spectrum shows the presence of alkane groups, firmly stretched around  $2915 \text{ cm}^{-1}$  and strong stretch vibration of carboxylic around  $1732 \text{ cm}^{-1}$ . Then C-O incorporated carboxylic group at  $1238$  and  $1173 \text{ cm}^{-1}$ . The bands around  $2915, 2850, 1471 \text{ cm}^{-1}$  show the presence of strong stretching of alkane groups. The spectrum of the produced biodiesels exhibits asymmetric and symmetric carboxylic group with strongly stretch vibration from  $2500$  to  $3000 \text{ cm}^{-1}$  as well as alcohol bonded with hydroxyl (broad OH stretching) between  $3500$  and  $3300 \text{ cm}^{-1}$ , which include alcohol and phenols group. The spectrum reveals the presence of ketones, aldehyde in conjunction with carboxylic group, and strong stretching of ester group between  $1471$  and  $1746 \text{ cm}^{-1}$  band. The  $1746 \text{ cm}^{-1}$  band is a major characteristic peak for both vegetable oils and their corresponding fatty acid methyl esters. The progress of the transesterification reaction could be monitored around  $1446\text{--}1428 \text{ cm}^{-1}$  [38], representing the methyl (O-CH<sub>3</sub>) peak ( $1436 \text{ cm}^{-1}$ ) (Fig. 5(b)). Fig. 5(b) reveals that SHY has the best yield, followed by ALK and HY and NaLK, the least. The spectrum around  $1030\text{--}1246 \text{ cm}^{-1}$  shows the presence of C-O together with the carboxylic and strong stretching of the ester group. The band around  $1362\text{--}1464 \text{ cm}^{-1}$  indicates the presence of strongly stretch alkane groups. The number and strength of Bronsted acid sites of the

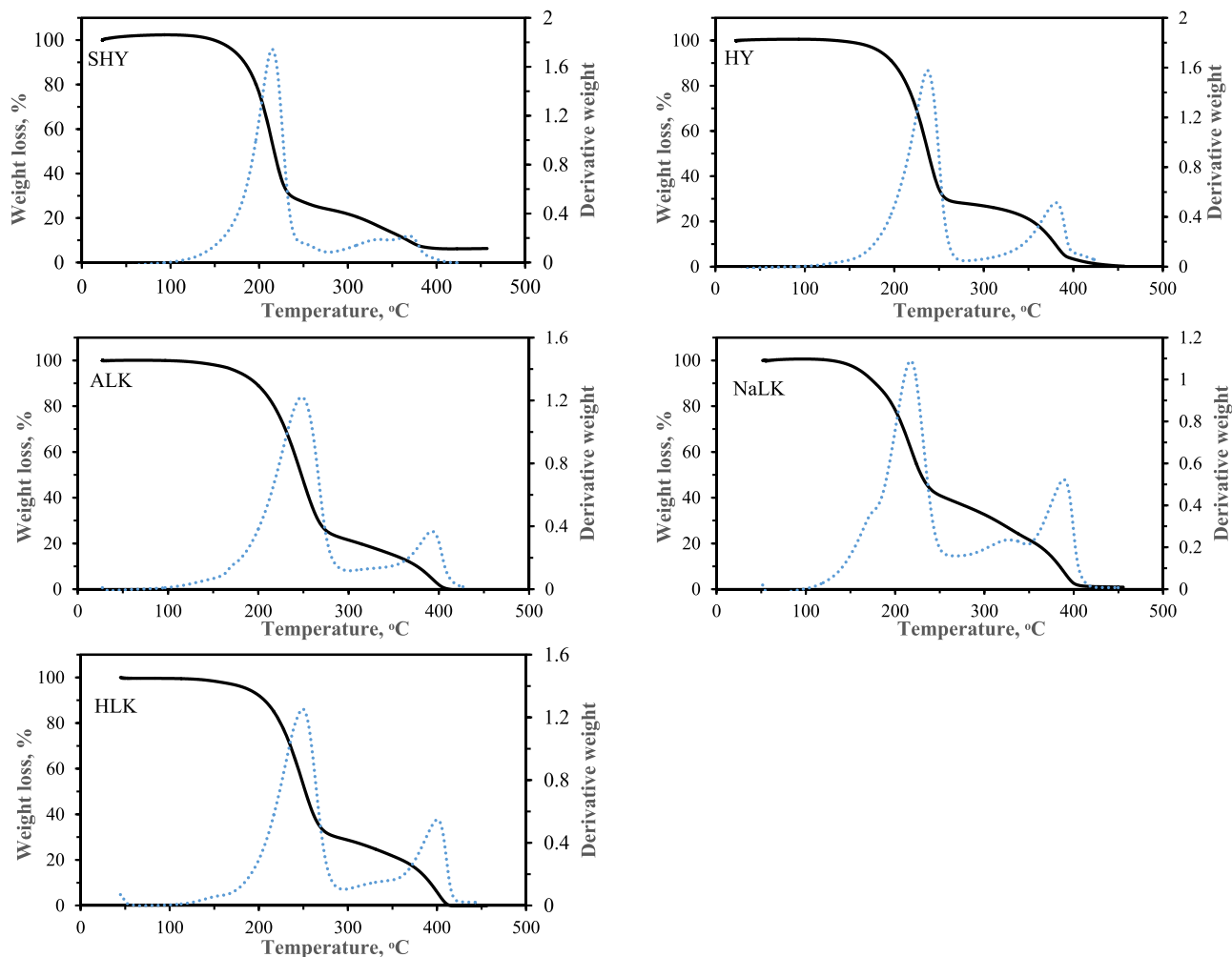


Fig. 7. TG curves of shea butter and biodiesel samples.

**Table 4**  
DTG decomposition characteristics of shea butter and biodiesel samples.

Sample	Reaction Region	Peak Temp	Weight loss %
Shea butter	146–298	255.08	8.36
SHY	145–279	218.08	90.76
HY	148–274	240.62	72.42
ALK	163–298	253.47	78.22
NaLK	133–264	220.48	80.15
HLK	168–295	253.43	79.18

**Table 5**  
Comparing the results of this work with previous report of biodiesel production from shea butter using 1 wt% catalyst, 5:1 MeOH/oil, at 200 C for 6 h.

Catalyst	Yield (%)	Ref
ZSM-5	57.49	[23]
0.3HMZeol	56.10	[23]
0.4HMZeol	78.45	[23]
HY	72.42	This work
SHY	90.76	This work
ALK	78.22	This work
HLK	79.18	This work
NaLK	80.15	This work

0.3HMZeol: ZSM-5 desilicated using 0.3 M NaOH,  
0.4HMZeol: ZSM-5 desilicated using 0.4 M NaOH.

catalyst are found around  $3300\text{--}3500\text{ cm}^{-1}$ , which is the broad O-H stretching. This result agrees with the reports of Farag et al. [2] and Ndana et al. [39].

### 3.5. TG/DTG analysis of shea butter and biodiesels

Fig. 6 gives the TG and DTG curves of the shea butter sample. Shea butter decomposes in two steps, as shown in the DTG curve, with the first being a small peak and the second is long. The former is attributed to the decomposition of bulky/unsaturated triglyceride molecules, and the latter is due to the complete devolatilization of shea butter. Similarly, the degradation of the biodiesel produced from all the catalyst samples proceeds in a two-step, as shown in the TG and DTG curves in Fig. 7. The first peak reveals the total decomposition of biodiesel, while the second peak is for the degradation of unreacted shea butter. Table 4 presents the DTG degradation characteristics of the biodiesel and shea butter samples. The DTG peak temperature of the samples could be used to determine thermal stability [26]. The samples thermal stability is in the order of  $\text{ALK} > \text{HLK} > \text{NaLK} > \text{HY} > \text{SHY}$ , while the samples biodiesel yield is in the order of  $\text{HY} < \text{ALK} < \text{HLK} < \text{NaLK} < \text{SHY}$ . The results reveal that modified kaolinates produce biodiesels with superior thermal stability when compared with zeolites. However, the zeolites performed better in terms of biodiesel yield except for ALK, which performed better than HY zeolites. The TGA yield results agree well with the observations from the FTIR spectrum (Fig. 6(b)). Moreover, acidity plays a vital role in the yield of biodiesel. As shown in Table 5, the results of the kaolin-based catalysts are similar to our previous report using ZSM-5

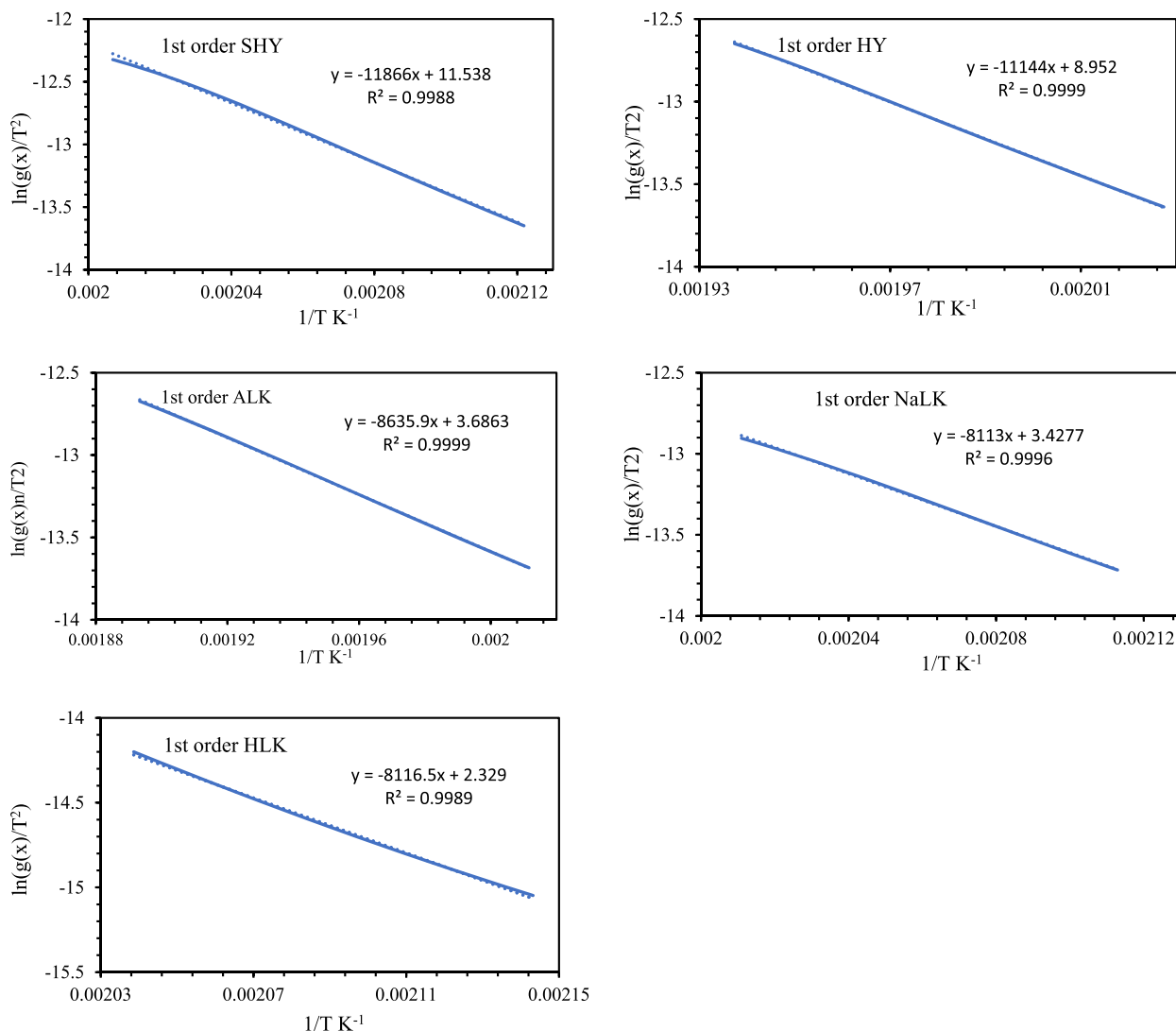


Fig. 8. Plot of  $\ln(g(x)/T^2)$  vs.  $1/T$  for all the biodiesel samples.

Table 6

TGA/DTG Conversion, Activation energies ( $E_A$ , kJ/mol) and pre-exponential factor ( $A$ ,  $\text{min}^{-1}$ ) of biodiesel samples according to first order model.

Sample	First order			Second order			Third order		
	EA	A	R2	EA	A	R2	EA	A	R2
SHY	98.65	2.55E+07	0.9988	132.92	2.23E+11	0.9991	173.41	9.68E+15	0.9957
HY	92.65	1.72E+06	0.9999	121.11	2.62E+09	0.9999	154.15	1.19E+13	0.996
ALK	71.80	6.89E+03	0.9999	94.40	2.41E+06	0.9988	120.64	1.97E+09	0.996
NaLK	67.45	5.00E+03	0.9996	83.67	4.28E+05	0.9998	101.95	6.09E+07	0.9991
HLK	67.48	1.67E+03	0.9989	71.45	5.05E+03	0.9984	75.56	1.58E+04	0.9978

and desilicated ZSM-5 and sulfated zeolite as catalyst and TGA for quantification at the same reaction conditions [23].

### 3.6. Kinetics analysis

Fig. 8 and Table 6 present the TG/DTG kinetic parameters of the produced biodiesel samples obtained from pyrolysis curves with their respective  $R^2$  values. The kinetic models were developed using the TG data using Microsoft Excel spreadsheet in modeling the data obtained from the thermographic analysis, following the Coats and Redfern model described in Section 2.7. The mechanism was explored using first, second and third-order reaction model to examine the best mechanism suitable for the process. The linear part of the reaction regions of the TG

plots was used. The slopes and intercept of the linear plots were utilized to determine the values of  $E_A$  and pre-exponential factor ( $A$ ) for each sample, as presented in Table 6. The pre-exponential factor is also known as the frequency factor, which depends on the frequency of collision of molecules when all concentrations are 1 mol/L. It also depends on the orientation of the molecules when they collide. Generally, the value of  $E_A$  varies  $A$  for a particular material. For the mesoporous aluminosilicates (ALK, NaLK, and HLK), the value of  $E_A$  is inversely related with  $A$ . Similarly, for SHY and HY,  $E_A$  decreases with an increase in  $A$ . Considering the  $E_A$  values of the biodiesel samples, the  $E_A$  value is in the order of SHY > HY > ALK > HLK > NaLK. This shows that SHY zeolite (98.65 kJ/mol) produced biodiesel exhibits the best stability, while ALK shows the least since the stability decrease with declining  $E_A$  [40].

Hence, more heat is needed for the SHY zeolite-produced biodiesel sample to be oxidized than other zeolites and modified kaolinites. While high acidity favors zeolites stability, the lower  $E_A$  of NaLK (67.45 kJ/mol) is due to higher basicity when compared to the other modified kaolinites. However, ALK shows the higher stability due to higher acidity. This reveals that  $E_A$  is a direct function of acidity for both the zeolites and the modified kaolinites.

#### 4. Conclusion

Viable aluminosilicate catalysts had been synthesized following different methodologies, and the performances were compared during biodiesel production from shea butter using TG/DTG and the stability of the produced biodiesels using degradation kinetic parameters. SHY zeolite was synthesized by sulfation of HY zeolite (produced from kaolin-based mesoporous aluminosilicate, ALK) to enhance the acidity and the pore structure of the sample for effective transesterification of shea butter. SHY zeolite exhibited better catalytic performance in biodiesel synthesis when compared with HY zeolite and the modified kaolinites (HLK, NaLK and ALK). Despite the sharp decline in the pore volume ( $0.23\text{--}0.06\text{ cm}^3\text{ g}^{-1}$ ) and SSA ( $444\text{--}66\text{ m}^2\text{ g}^{-1}$ ), SHY leveraged on the improved pore size (which boosts diffusion of FAME), and the effect of functionalization with sulfate ion to exhibit a superior activity.

Comparing the performance of all the catalysts, the stability of the biodiesels produced from catalyst samples is in the order of SHY>HY>ALK>HLK>NaLK, while the samples biodiesel yield is in the order of HY<ALK<HLK<NaLK<SHY. Sulfate-modified zeolite produces biodiesels with superior thermal stability when compared with the modified kaolinites. Moreover, the sulfate ion modified zeolite performed better in terms of biodiesel yield followed by NaLK, which performed better than HY zeolite and other modified kaolinites. SHY zeolite is the best catalyst based on the yield (91%), and stability. The findings of this study will be useful for both researchers and industrial players towards producing biodiesel with enhanced physical and oxidative stability.

#### CRedit authorship contribution statement

**Faisal Abnisa:** Conceive and design analysis, Wrote the paper. **Eshorame Samuel Sanni:** Collect data, Perform analysis, Revised the manuscript. **Peter Adeniyi Alaba:** Perform the experiment, Collect data, Performed the modeling of the kinetic parameters.

#### Declaration of Competing Interest

The authors declare that they have no known competing financial interests or personal relationships that could have appeared to influence the work reported in this paper.

#### Acknowledgments

This project was funded by the Deanship of Scientific Research (DSR), King Abdulaziz University, Jeddah, under grant No. (G: 836-829-1441). The authors, therefore, gratefully acknowledge DSR technical and financial support.

#### References

- I. Mohammed, F. Kazi, S. Yusup, P. Alaba, Y. Sani, Y. Abakr, Catalytic intermediate pyrolysis of napier grass in a fixed bed reactor with ZSM-5, HZSM-5 and zinc-exchanged zeolite-A as the catalyst, *Energies* 9 (2016) 246.
- H. Farag, A. El-Maghraby, N.A. Taha, Transesterification of esterified mixed oil for biodiesel production, *Int. J. Chem. Biochem. Sci.* 2 (2012) 105–114.
- D. Reinoso, D. Damiani, G. Tonetto, Synthesis of biodiesel from soybean oil using zinc layered hydroxide salts as heterogeneous catalysts, *Catal. Sci. Technol.* 4 (2014) 1803–1812.
- A. Carrero, G. Vicente, R. Rodríguez, M. Linares, G. Del Peso, Hierarchical zeolites as catalysts for biodiesel production from *Nannochloropsis* microalga oil, *Catal. Today* 167 (2011) 148–153.
- Y.M. Sani, P.A. Alaba, A.O. Raji-Yahya, A.A. Aziz, W.M.A.W. Daud, Facile synthesis of sulfated mesoporous Zr/ZSM-5 with improved Brønsted acidity and superior activity over SZr/Ag, SZr/Ti, and SZr/W in transforming UFO into biodiesel, *J. Taiwan Inst. Chem. Eng.* 60 (2016) 247–257.
- P.A. Alaba, Y.M. Sani, S.F. Olupinla, W.M.W. Daud, I.Y. Mohammed, C. C. Enweremadu, O.O. Ayodele, Toward N-nitrosamines free water: formation, prevention, and removal, *Crit. Rev. Environ. Sci. Technol.* 47 (2017) 2448–2489.
- P.A. Alaba, N.A. Oladoja, Y.M. Sani, O.B. Ayodele, I.Y. Mohammed, S.F. Olupinla, W.M.W. Daud, Insight into wastewater decontamination using polymeric adsorbents, *J. Environ. Chem. Eng.* 6 (2018) 1651–1672.
- G.A. Adebisi, Z.Z. Chowdhury, P.A. Alaba, Equilibrium, kinetic, and thermodynamic studies of lead ion and zinc ion adsorption from aqueous solution onto activated carbon prepared from palm oil mill effluent, *J. Clean. Prod.* 148 (2017) 958–968.
- P.A. Alaba, Y.M. Sani, W.M.A.W. Daud, Efficient biodiesel production via solid superacid catalysis: a critical review on recent breakthrough, *RSC Adv.* 6 (2016) 78351–78368.
- J. Čejka, G. Centi, J. Perez-Pariente, W.J. Roth, Zeolite-based materials for novel catalytic applications: opportunities, perspectives and open problems, *Catal. Today* 179 (2012) 2–15.
- H. Konno, T. Tago, Y. Nakasaka, R. Ohnaka, J.-I. Nishimura, T. Masuda, Effectiveness of nano-scale ZSM-5 zeolite and its deactivation mechanism on catalytic cracking of representative hydrocarbons of naphtha, *Microporous Mesoporous Mater.* 175 (2013) 25–33.
- Y. Yu, X. Li, L. Su, Y. Zhang, Y. Wang, H. Zhang, The role of shape selectivity in catalytic fast pyrolysis of lignin with zeolite catalysts, *Appl. Catal. A Gen.* 447 (2012) 115–123.
- A.J. Foster, J. Jae, Y.-T. Cheng, G.W. Huber, R.F. Lobo, Optimizing the aromatic yield and distribution from catalytic fast pyrolysis of biomass over ZSM-5, *Appl. Catal. A Gen.* 423 (2012) 154–161.
- J. Li, X. Li, G. Zhou, W. Wang, C. Wang, S. Komarneni, Y. Wang, Catalytic fast pyrolysis of biomass with mesoporous ZSM-5 zeolites prepared by desilication with NaOH solutions, *Appl. Catal. A Gen.* 470 (2014) 115–122.
- A. Ishihara, K. Kimura, A. Owaki, K. Inui, T. Hashimoto, H. Nasu, Catalytic cracking of VGO by hierarchical ZSM-5 zeolite containing mesoporous silica-aluminas using a curie point pyrolyzer, *Catal. Commun.* 28 (2012) 163–167.
- R.K. Saluja, V. Kumar, R. Sham, Stability of biodiesel—A review, *Renew. Sustain. Energy Rev.* 62 (2016) 866–881.
- L. Das, D.K. Bora, S. Pradhan, M.K. Naik, S. Naik, Long-term storage stability of biodiesel produced from Karanja oil, *Fuel* 88 (2009) 2315–2318.
- G. Knothe, R.O. Dunn, Dependence of oil stability index of fatty compounds on their structure and concentration and presence of metals, *J. Am. Oil Chem. Soc.* 80 (2003) 1021–1026.
- S. Nisar, U. Farooq, F. Idress, U. Rashid, T.S.Y. Choong, A. Umar, Biodiesel by-product glycerol and its products, *Int. J. Chem. Biochem. Sci.* 9 (2016) 92–96.
- R.O. Dunn, Effect of temperature on the oil stability index (OSI) of biodiesel, *Energy Fuels* 22 (2008) 657–662.
- I.Y. Mohammed, Y.A. Abakr, S. Yusup, P.A. Alaba, K.I. Morris, Y.M. Sani, F.K. Kazi, Upgrading of Napier grass pyrolytic oil using microporous and hierarchical mesoporous zeolites: products distribution, composition and reaction pathways, *J. Clean. Prod.* 162 (2017) 817–829.
- M. Lenarda, L. Storaro, A. Talon, E. Moretti, P. Riello, Solid acid catalysts from clays: preparation of mesoporous catalysts by chemical activation of metakaolin under acid conditions, *J. Colloid Interface Sci.* 311 (2007) 537–543.
- P.A. Alaba, Y.M. Sani, I.Y. Mohammed, Y.A. Abakr, W.M.A.W. Daud, Synthesis and application of hierarchical mesoporous HZSM-5 for biodiesel production from shea butter, *J. Taiwan Inst. Chem. Eng.* 59 (2016) 405–412.
- P.A. Alaba, Y.M. Sani, I.Y. Mohammed, Y.A. Abakr, W.M.A.W. Daud, Synthesis and characterization of sulfated hierarchical nanoporous faujasite zeolite for efficient transesterification of shea butter, *J. Clean. Prod.* 142 (2017) 1987–1993.
- P.A. Alaba, Y.M. Sani, W.M.A.W. Daud, Synthesis and characterization of hierarchical nanoporous HY zeolites from acid-activated kaolin, *Chin. J. Catal.* 36 (2015) 1846–1851.
- P.A. Alaba, S.I. Popoola, F. Abnisa, C.S. Lee, O.S. Ohunakin, E. Adetiba, M. B. Akanle, M.F.A. Patah, A.A. Atayero, W.M.A.W. Daud, Thermal decomposition of rice husk: a comprehensive artificial intelligence predictive model, *J. Therm. Anal. Calorim.* 140 (2019) 1811–1823.
- E.A. Williams, P.T. Williams, Analysis of products derived from the fast pyrolysis of plastic waste, *J. Anal. Appl. Pyrolysis* 40–41 (1997) 347–363.
- P. Chand, C.V. Reddy, J.G. Verkade, T. Wang, D. Grewell, Thermogravimetric quantification of biodiesel produced via alkali catalyzed transesterification of soybean oil, *Energy Fuels* 23 (2009) 989–992.
- P.A. Alaba, Y.M. Sani, W.M.A.W. Daud, A comparative study on thermal decomposition behavior of biodiesel samples produced from shea butter over micro-and mesoporous ZSM-5 zeolites using different kinetic models, *J. Therm. Anal. Calorim.* 126 (2016) 943–948.
- I.Y. Mohammed, Y.A. Abakr, J.N.X. Hui, P.A. Alaba, K.I. Morris, M.D. Ibrahim, Recovery of clean energy precursors from Bambara groundnut waste via pyrolysis: kinetics, products distribution and optimisation using response surface methodology, *J. Clean. Prod.* 164 (2017) 1430–1445.
- E. Apaydin-Varol, S. Polat, A.E. Putun, Pyrolysis kinetics and thermal decomposition behavior of polycarbonate—a TGA-FTIR study, *Therm. Sci.* 18 (2014) 833–842.

- [32] O.B. Ayodele, Effect of phosphoric acid treatment on kaolinite supported ferrioxalate catalyst for the degradation of amoxicillin in batch photo-Fenton process, *Appl. Clay Sci.* 72 (2013) 74–83.
- [33] P. Hu, H. Yang, Insight into the physicochemical aspects of kaolins with different morphologies, *Appl. Clay Sci.* (2012).
- [34] A.K. Panda, B. Mishra, D. Mishra, R. Singh, Effect of sulphuric acid treatment on the physico-chemical characteristics of kaolin clay, *Colloids Surf. A Physicochem. Eng. Asp.* 363 (2010) 98–104.
- [35] P.A. Alaba, Y.M. Sani, W.M.A.W. Daud, Kaolinite properties and advances for solid acid and basic catalyst synthesis, *RSC Adv.* 5 (2015) 101127–101147.
- [36] M. Chmielová, Z. Weiss, Determination of structural disorder degree using an XRD profile fitting procedure. Application to Czech kaolins, *Appl. Clay Sci.* 22 (2002) 65–74.
- [37] P. Ptáček, T. Opravil, F. Šoukal, J. Wasserbauer, J. Másilko, J. Baráček, The influence of structure order on the kinetics of dehydroxylation of kaolinite, *J. Eur. Ceram. Soc.* 33 (2013) 2793–2799.
- [38] W.-B. Zhang, Review on analysis of biodiesel with infrared spectroscopy, *Renew. Sustain. Energy Rev.* 16 (2012) 6048–6058.
- [39] M. Ndana, J. Grace, F. Baba, U. Mohammed, Fourier transform infrared spectrophotometric analysis of functional groups in biodiesel produced from oils of *Ricinus communis*, *Hevea brasiliensis* and *Jatropha curcas* seeds, *Int. J. Sci. Environ. Technol.* 2 (2013) 1116–1121.
- [40] A. Souza, H. Danta, M.C. Silva, I.M. Santos, V. Fernandes, F.S. Sinfrônio, L. S. Teixeira, C. Novák, Thermal and kinetic evaluation of cotton oil biodiesel, *J. Therm. Anal. Calorim.* 90 (2007) 945–949.